Colloids and Surfaces B: Biointerfaces 88 (2011) 354–361

Contents lists available at ScienceDirect

Colloids and Surfaces B: Biointerfaces

journal homepage: www.elsevier.com/locate/colsurfb

Keratin capped silver nanoparticles – Synthesis and characterization of a nanomaterial with desirable handling properties

Justin J. Martin*, Jeanette M. Cardamone, Peter L. Irwin, Eleanor M. Brown

U.S. Department of Agriculture, Agricultural Research Service, Eastern Regional Research Center, 600 East Mermaid Lane, Wyndmoor, PA 19038, USA

ARTICLE INFO

Article history:
Received 25 March 2011
Received in revised form 3 June 2011
Accepted 5 July 2011
Available online 21 July 2011

Keywords:
Nanoparticle
Antimicrobial
Silver
Keratin
Wool
Biocompatible

ABSTRACT

We report for the first time the stabilization of silver nanoparticles in good yield, average diameter 3.5 nm, using wool keratin hydrolysates as stabilizers. The nanoparticles are extremely stable as a suspension and can be lyophilized into a powder and easily reconstituted in solvent with no change in spectral properties relative to the initial suspension. The nanoparticles interact with nitrogen and oxygen moieties of the keratin hydrolysates under the pH conditions used in the synthesis and appear to act as cross-linkers between adjacent chains. The product has excellent handling properties which we believe will make it a very attractive biocompatible coating/additive, providing prolonged antimicrobial efficacy to a wide variety of products such as textiles, plastics, paints, orthopedic devices and others.

1. Introduction

Over the past several years, interest in developing advanced materials using components originating or derived from proteins and other natural products has expanded significantly. This interest is partly fueled by innovation in the medicinal sciences, fueled by a constant need for novel approaches to tissue engineering, implantation devices (and coatings for these devices), as well as creating biologically active surfaces [1]. The drive toward green solutions in the chemical industry has also fueled interest in the responsible utilization of natural products. We have been investigating the use of protein-based materials from underutilized agricultural by-products for textile applications and as stand alone products either "as-is" or after further reactivity [2]. In particular, we have been interested in developing keratin obtained from wool as a pure protein prototype material to evaluate the potential utilization of keratinaceous waste as a source for a biocompatible nanoparticle stabilizer.

Keratin, the major component of hair, feathers, and the horns and nails of mammals, reptiles and birds is an abundant protein. It is estimated that keratin waste from industrial processes such as the wool and meat industries is in excess of 3 million tonnes per year [1]. Other researchers examining keratin derivatives isolated from wool have shown that the extracted material exhibits excellent biocompatibility and may promote cellular growth [3,4].

One exciting area that we wanted to explore for the utility of soluble keratin capping agents is that of integrating textiles with functional inorganic nanoparticles. Inorganic nanoparticles are known to exhibit size and shape dependent properties [5–8]. Traditionally, these properties have been exploited primarily for various sensors, catalysis, optics, data storage and light emitting diodes [5–8]. Researchers have established the utility of nanoparticles as potent antimicrobials as well. Recent studies have indicated that spherical silver nanoparticles capped by citrate are capable of disrupting the cellular membrane of several pathogenic microorganisms, leading to collapse of the plasma membrane potential resulting in death [9,10]. The efficacy of silver nanoparticles against a wide range of microbes has inspired scientists to look for cost-sensitive and efficient methods for attaching them to textiles and many other materials while not interfering with their efficacy. Though well-studied, the ubiquitous citrate capped silver nanoparticle shows little affinity to wool or cotton without the use of harsh chemicals or pre-treatments that often have a severe effect on desirable intrinsic properties of the textile or polymeric substrate. Poor adhesion of nanoparticles to the substrate or poor dispersion within coatings are engineering concerns that must be addressed for adoption of antimicrobial silver technology. Keratin's intrinsic chemistry offers an attractive opportunity to stabilize a multitude of inorganic nanoparticles. Previous studies have demonstrated a strong affinity between keratin and metal cations/metals

* Corresponding author. Tel.: +1 607 761 4665.
E-mail address: householdbleach@yahoo.com (J.J. Martin).

0927-7765/$ – see front matter © 2011 Elsevier B.V. All rights reserved.
doi:10.1016/j.colsurfb.2011.07.013

including gold, copper, silver, iron, cadmium, lead, chromium, sodium, mercury and aluminum [11]. Furthermore, the aromatic tyrosine and phenylalanine residues, peptide bonds, sulfur groups from cysteine residues, free amines, free carboxylate groups, amides and other functionalities offer materials chemists tremendous synthetic utility for adsorption to a large number of materials while allowing future reactivity. The secondary structure of keratin can vary depending on the source. The alpha helix is the principal structural unit found in wool fibers, which were used to generate the capping agent in this study.

In a previous study, we were the first to suggest the use of wool keratin hydrolysates as particle carriers/capping agents for textile integration [2d]. In this follow-up study, we report our reproducible synthesis combined with characterization, stability and handling properties of wool keratin stabilized silver nanoparticles possessing desirable commercial properties [2d]. The nanomaterials described herein can be easily redispersed from a powder, allowing their use in a wide variety of coatings or coating formulations.

2. Materials and methods

2.1. Preparation of keratin hydrolysates

Scoured and carbonized wool fibers, ~21 μm were supplied from the Bollman Hat Company, Adamstown, PA and were used for preparing wool keratin hydrolysates following a cleaning step in which methylene chloride was passed over the wool in a Soxhlet extractor. The cleaned wool was added to a 0.5 N NaOH solution at 60 °C for 3 h according to a previously published procedure to produce the keratin hydrolysates [2]. The hydrolysates were dialyzed through 6000–8000 Da MWCO Spectrapor dialysis tubing with three water changes over a 24-h period and lyophilized using a FTS FlexiDry™ instrument.

2.2. Preparation of silver nanoparticles

Silver nitrate, sodium citrate and sodium borohydride were purchased from Aldrich and used as received. De-ionized (DI) water (>18 MΩ resistance) was obtained using a Barnstead Nanopure filtration system. Keratin stabilized nanoparticles were produced by measuring approximately 0.100 g of Bollman keratin hydrolysate and adding it to 100 mL of rapidly stirring DI water. The pH of the solution is important and changed from 5.6 (DI water) to 8.5–8.9 upon addition of the keratin hydrolysate. Dilute sodium hydroxide was added to achieve a pH in the range of 8.5–8.9 if pH was not measured to be within this range after addition of keratin hydrolysate. This is necessary to buffer the solution from the pH drop upon addition of silver nitrate. After allowing approximately five minutes for all of the material to be completely dissolved, 0.184 g (~1.0×10^{-3} mol) of silver nitrate were added and allowed to stir rapidly for approximately 5 min. Upon addition of the silver nitrate, the pH typically changed to 6.7. In a separate vial, 0.0097 g (~2.5×10^{-3} mol) of sodium borohydride was measured and added to 5 mL of DI water. Exactly 1 mL of this solution was added dropwise to the rapidly stirring keratin/silver nitrate solution over the course of 10 min. The solution darkened to a dark orange color and the final pH of the solution was typically measured to be 7.7. Deviation from this preparation either by decreasing the protein concentration or increasing the silver and $NaBH_4$ concentration resulted in a completely insoluble orange colored precipitate with excellent film forming properties when dried. We believe this precipitation to be a result of enhanced cross-linking and increased silver nucleation/Ostwald ripening at higher silver to stabilizer ratios and will be the subject of a future study. Keratin capped silver nanoparticle hydrolysates were lyophilized under the same conditions as those reported for keratin hydrolysates.

2.3. Characterization of silver nanoparticles

TEM images were recorded using a Philips CM12 Cryo system from dilute solutions. The TEM micrographs were analyzed using ImageJ software. This software has convenient tools to allow statistical analysis and measurement of features present in digital images. UV–vis measurements of the surface plasmon resonance (SPR) band were recorded in solution using a Cary 50 spectrophotometer, a Tecan Microplate Reader equipped with XFluor4SafireII software v4.62A (100 averages) and an Aviv instruments UV–vis spectrophotometer model 14NT-UV–vis. Circular dichroism spectroscopy was performed using an Aviv Instruments CD spectrometer model 215 using 1 mm pathlength cells under the following conditions (25 °C, λ_{range} = 190–320, 1 nm step, 2 s average time). Fourier transform infrared spectroscopy was performed using a Nicolet Magna spectrometer equipped with a mercury cadmium telluride detector. The instrument was run in transmission mode with a scanning range of 3500 cm^{-1} to 400 cm^{-1} with a 1 cm^{-1} resolution and a minimum of 1024 averages. Lyophilized powders of both the Bollman keratin and the Bollman keratin stabilized nanoparticles were added to an excess of KBr and pressed into a transparent window for analysis.

2.4. Molecular weights and amino acid composition

Molecular weights were estimated using gel electrophoresis SDS-PAGE on an Amersham Biosciences Phast system according to a previously published procedure [2]. A keratin hydrolysate control, a molecular weight standard solution (Bio-Rad Broad Range Standard) and the silver nanoparticle sample were loaded on 4–15% gradient gels. After electrophoresis, gels were stained with Coomassie brilliant blue R-250 and destained. Amino acid analysis was performed using a previously published procedure [2].

3. Results and discussion

3.1. Molecular weight determination and amino acid analysis

Previous studies using gel electrophoresis have determined that the molecular weight distribution for wool keratin solubilized with NaOH under severe hydrolysis conditions is 6.5–21 kDa [2]. Assuming a mean residue weight of 111.8, the chain lengths of the solubilized keratins are at most 100–200 amino acids in length. The SDS-PAGE for the materials prepared and used in this study is shown in Fig. 1.

Our results suggest that the predominant molecular weight fraction for the hydrolyzed keratin capping agent (control) is 6.5 kDa or below. When the keratin is stabilized with silver nanoparticles, a significant molecular weight fraction >250 kDa is seen. We attribute this dramatic increase in molecular weight to silver nanoparticle(s) bridging keratin hydrolysate segments and/or multiple hydrolysate molecules behaving as a capping agent. We do not attribute this to disulfide bridges forming between cysteine moieties on adjacent chains as the band is not seen in the control (KH) and the presence of a strong reducing agent during synthesis should discourage disulfide bridge formation.

The amino acid composition of the Bollman wool fiber (Table 1) was consistent with the composition of wool fiber reported earlier by Freddi et al. [12]. The alkaline hydrolyzed samples [2a] showed significant losses of serine, threonine and arginine. Cysteine was either completely lost or below the detection limit.

Notably, cysteine forms the disulfide bridges that hold the native keratin together. Furthermore, in its reduced form, the thiol

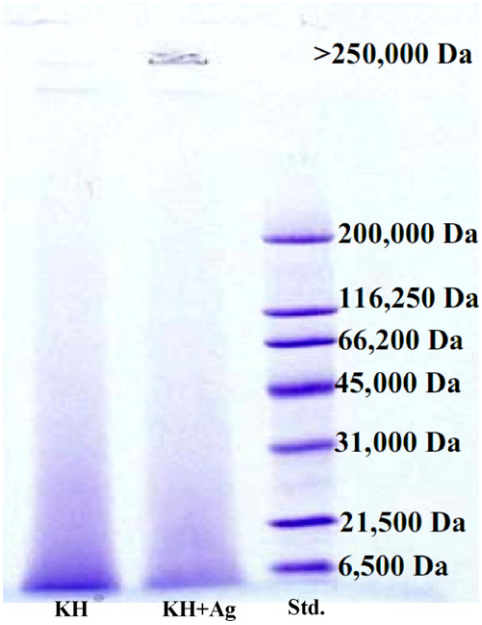

Fig. 1. SDS-PAGE of keratin hydrolysate (KH, far left), keratin stabilized nanoparticles (KH + Ag middle) and molecular weight standard (Std., far right).

presents an attractive site for noble metal bonding. Previous studies have shown that severe alkaline hydrolysis leads to hydroxide ion catalyzed β-elimination of the disulfide group in cysteine [13,14]. The elimination of the disulfide bond can be a driving force in achieving protein solubility via alkaline hydrolysis. It appears that the conditions used to facilitate this process have led to a profound decrease in the availability of cysteine sulfur moieties. For the synthesis of silver nanoparticles using this material as a stabilizer, this finding is significant as silver/silver oxide has long been shown to have a strong affinity to sulfur lone pairs such as those present in thiols [15]. The method used to determine the amino acid content results in the hydrolysis of glutamine to glutamic acid and asparagine to aspartic acid.

3.2. FT-IR

The FT-IR spectrum for alkaline hydrolyzed keratin shows peak structure primarily attributed to peptide bonds and methyl groups. The modes associated with peptide bonds (–CONH–) give rise to

Table 1
Amino acid comparison of untreated wool and solubilized wool keratin. The Freddi reference is given for comparison.

Amino acid	Untreated wool (mol%) [12]	Untreated wool (mol%) [2a]	Soluble keratin (mol%) [2a]
Aspartic acid	6.43	7.36	11.3
Glutamic acid	12.23	13.1	20.8
Serine	11.0	10.9	4.0
Glycine	9.44	7.19	7.0
Histidine	0.80	0.66	0.80
Arginine	7.30	7.45	5.16
Threonine	6.38	6.63	2.47
Alanine	5.76	5.95	7.91
Proline	7.08	6.88	6.51
Tyrosine	3.51	3.1	3.81
Valine	6.38	6.47	7.57
Methionine	0.59	0.68	0.84
Cysteine	5.65	5.77	Not detectible
Isoleucine	3.45	3.69	4.82
Leucine	8.08	8.31	11.2
Phenylalanine	2.93	2.77	2.80
Lysine	3.01	3.04	3.03

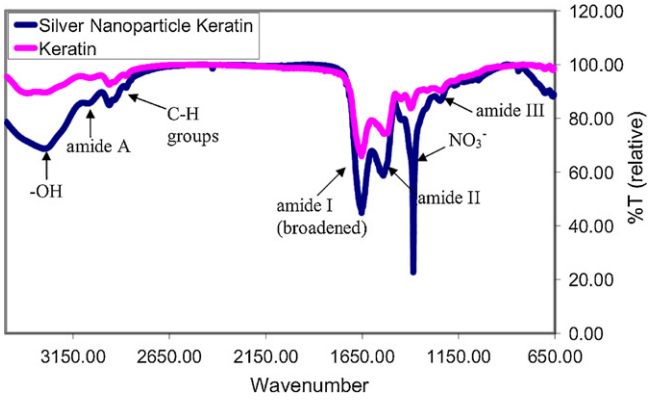

Fig. 2. FT-IR spectra with summary for keratin and nanoparticle keratin.

absorption regions known as amide A, and amide I,II,III. Amide A consists of N–H stretching modes and is a broad, higher frequency transition occurring at approximately 3282 cm^{-1}. Amide I consists predominantly of the C=O stretching vibrational mode and typically falls between 1600 and 1700 cm^{-1}. Amide II, typically occurs around 1520 cm^{-1} and results from N–H bending and C–H stretching vibrations. Amide III, typically occurring between 1220 and 1300 cm^{-1}, is a complex absorption arising from in phase combinations of C–N stretching and N–H in plane bending as well as C–C stretching and C=O bending vibrations [1,2]. The modes associated with methyl groups primarily occur between 2880 and 2970 cm^{-1}. These spectra are shown in Fig. 2.

Because we cannot directly observe silver metal vibrations using FT-IR, shifts in the vibrational frequency for binding sites such as those relating to Lewis base moieties can provide information about the interaction of silver with the keratin stabilizer. This analysis is complicated due to the presence of sodium ions used in processing the solubilized material and from the reduction. However, because the keratin used to produce the silver nanoparticles is the same as the keratin control, shifts in the infrared spectrum relating to Lewis basic (amide, hydroxyl) functional groups after nanoparticle formation are not believed to be sodium related. Fig. 2 summarizes the amide regions maximum absorption for both the extracted keratin and keratin stabilized nanoparticles.

The results in Fig. 2 show that only the amide frequencies primarily corresponding to nitrogen vibrational modes (amide A, amide II and amide III) show a distinct shift in wavenumber. Furthermore, the –OH region was observed to shift upon formation of silver nanoparticles. All of the observed peak shifts led to increases in wavenumber for the mode, a finding consistent with previously reported formation of silver nanorods in the protein bovine serum albumin (BSA) [16]. The observed shifts were not as distinct as those reported with BSA. We attribute this finding to the presence of sodium. Under severe alkaline hydrolysis conditions, sodium hydroxide can form carboxylate salts and can also form salts with phenols and hydrolyze amides to form sodium salts. In addition to shifts in wavenumber, the shape of the amide A/hydroxyl region appears different for the nanoparticle infused samples. This result is not surprising because nitrogen moieties are expected to have a strong affinity toward silver in this system as well as the lone pairs on oxygen and any remaining sulfur, though the sulfur containing cysteine residues appear to be minimal. Similar positive shifts in the wavenumber of vibrational modes corresponding to electron rich functionalities have been reported previously in polymer/nanoparticle hybrid materials [17–19]. The very intense peak at approximately 1384 cm^{-1} corresponds to NO_3 (nitrate) vibrational modes originating from the nitrate anion present as a dissociation product of silver nitrate [16]. For all of the silver

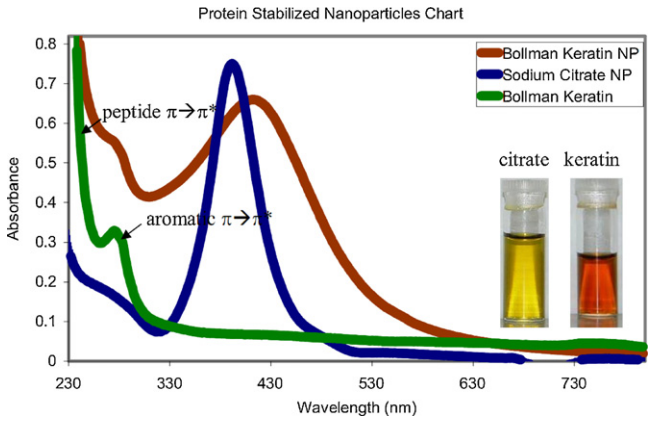

Fig. 3. UV–vis spectra of Bollman keratin, citrate stabilized nanoparticles and Bollman keratin stabilized nanoparticles.

nanoparticle keratin samples, a weak peak appears at 2428 cm^{-1} that is not present in the Bollman keratin sample. This peak was also present in previously published reports depicting the IR spectrum for silver nanorods prepared with BSA [16]. We are currently unable to offer a satisfactory explanation for this peak and this peak was not addressed in aforementioned studies. We also see minor broadening of the amide I region which has been attributed to capping of silver nanoparticles by proteins [20,21]. These results suggest that the amide region, in particular the nitrogen associated modes and hydroxyl groups are affected by the presence of silver and/or silver ions. Additional physical characterization methods such as UV–vis and TEM provide further evidence for the formation of stable capped silver nanoparticles.

3.3. UV–vis

The UV–vis spectrum for alkaline hydrolyzed keratin shows two noticeable absorptions. The most intense absorption, occurring at approximately 190 nm is related to the π–π* transition for the peptide bond. The lower energy transition, occurring at 274 nm, corresponds to the π–π* transition in the aromatic portion of tyrosine which has an extinction coefficient of 1400 M^{-1} cm^{-1} at this wavelength [22]. The peak was unaffected when lowering the pH of the solution to acidic conditions. Tyrosine, an amino acid that is well conserved through our processing, appears to be the only major contributor to this peak. If tryptophan were present, its extinction coefficient of 5700 M^{-1} cm^{-1} at 280 nm would shift the peak to a higher wavelength. The π–π* transition for the phenylalanine amino acid is symmetry forbidden and consequently has a much lower extinction coefficient, approximately 400 M^{-1} cm^{-1}, it cannot be resolved due to the intensity of the transitions for the peptide bonds. These transitions are shown in Fig. 3.

One of the characteristic indicators to the formation of inorganic nanoparticles is the presence of an intense peak ($\varepsilon \sim 107$ M^{-1} cm^{-1}) in the visible portion of the electromagnetic spectrum. This peak is a function of the free moving electrons across the nanoparticle surface and is known as Surface Plasmon Resonance (SPR). Because this is predominantly a surface phenomenon, the energy of this transition is highly dependent on the shape and the size of a given nanoparticle. For a colloidal sodium citrate stabilized silver nanoparticle sample, the maximum absorption for a 10 nm diameter particle occurs at ~389 nm with a shoulder appearing at higher energy. For silver nanoparticles stabilized with hydrolyzed wool keratin, the transition is broadened and red shifts to approximately 412 nm. This broadening is likely due to the polymeric nature of the stabilizer which allows some assembly of the individual nanoparticles. Similar broadening effects have been reported previously by groups such as Mirkin et al. when DNA was used to form nanoparticle assemblies [23]. An alternative explanation for the change in spectral properties may be a shift in the interfacial dielectric constant for a particle surrounded by water as opposed to surrounded in protein. The absorption spectra for both the traditionally prepared citrate stabilized nanoparticles and the keratin stabilized nanoparticles are shown in Fig. 3.

3.4. Circular dichroism spectroscopy

To obtain an understanding of the capping agent conformation and thus a better picture of the overall bonding environment, circular dichroism was performed on both the keratin hydrolysate and the capped nanoparticles. The keratin hydrolysate sample and the nanoparticle sample yielded very similar spectra, showing no evidence of ordered secondary structure (α-helix and β-sheet). In a protein possessing discrete secondary structure, the presence of a α-helical domain is indicated by the presence of a pair of intense peaks between 230 and 200 nm [22]. The β-sheet conformation is also indicated in this area. The large negative [θ] value for the peptide bond combined with a weak positive [θ] at lower energies is consistent with a disordered or random structural conformation [22]. Fig. 4 shows the CD curves for the keratin hydrolysate and the keratin capped nanoparticles as well as a comparison UV–vis spectrum recorded using the same samples. In general, the shape of the CD trace should appear consistent with the absorbance spectrum [22].

Clearly, the formation of silver nanoparticles does not result in an observable effect on the secondary structure of the keratin capping agent. The absence of secondary structure is likely a result of the alkaline hydrolysis processing conditions that were used to obtain a soluble keratin hydrolysate in this study. The absorbance at 214 nm, often used to estimate peptide bond concentration was 1.36 for the keratin solution and 1.44 for the solution of keratin capped nanoparticles suggesting that the peptide bond concentration is similar for both samples.

3.5. TEM

TEM analysis of the keratin stabilized nanoparticles revealed the presence of small, discrete spherical particles. These images are shown in Fig. 5. The keratin matrix limits the contrast that can be achieved in the TEM images. The nanoparticle measurements for the citrate stabilized and keratin stabilized nanoparticles show a unimodal size distribution with an average diameter of 3.5 nm ± 0.74 nm as shown in Fig. 5.

Further examination of the TEM grids, which had been treated with the keratin stabilized nanoparticles revealed the presence of rare nanoparticle assemblies showing a remarkable head/tail structure. The heads, which appeared to be constructed of several smaller silver nanoparticles and keratin filler had a diameter ranging from 10 to 100 nm. The tails appeared to be made up entirely of keratin and had a diameter of 2 nm (Fig. 5).

It is not clear at this time whether these aggregates are present in the colloidal suspension or if they are a drying phenomenon related to the preparation of the TEM samples. With the exception of locating these assembly structures, the nanoparticles appear to be remarkably well dispersed within the protein matrix with minimal agglomeration. This is a well known benefit to using synthetic polymeric materials as stabilizers in the preparation of inorganic nano-crystals [17]. Furthermore, the composition of the keratin polymeric chains have undoubtedly played an important role in limiting crystal growth during the reduction process. The ubiquitous sodium citrate method for producing metal nanoparticles, first described by Hauser and Lynn for gold systems and extended and modified for other noble metals, typically results in nanoparticles

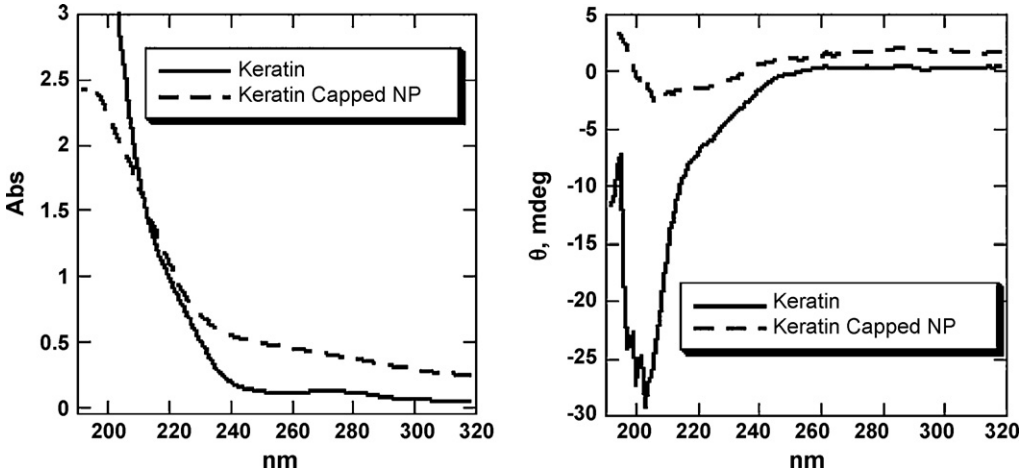

Fig. 4. Circular dichroism spectra for keratin hydrolysate and capped nanoparticles. The UV–vis spectrum is shown on the left for comparison.

with an average diameter ranging from 10 to 100 nm depending heavily on the reaction conditions [24,25]. The striking difference in size between the citrate capped nanoparticles and the keratin capped nanoparticles produced under the same experimental conditions demonstrates an obvious change in the crystallization kinetics for the macromolecular system as expected. In many cases, a recognition-reduction-limited nucleation and growth model can successfully explain the silver nanoparticle formation in the presence of a protein stabilizer [20,26–32]. In this model, silver ions are either chelated or held firmly in place on the protein backbone via

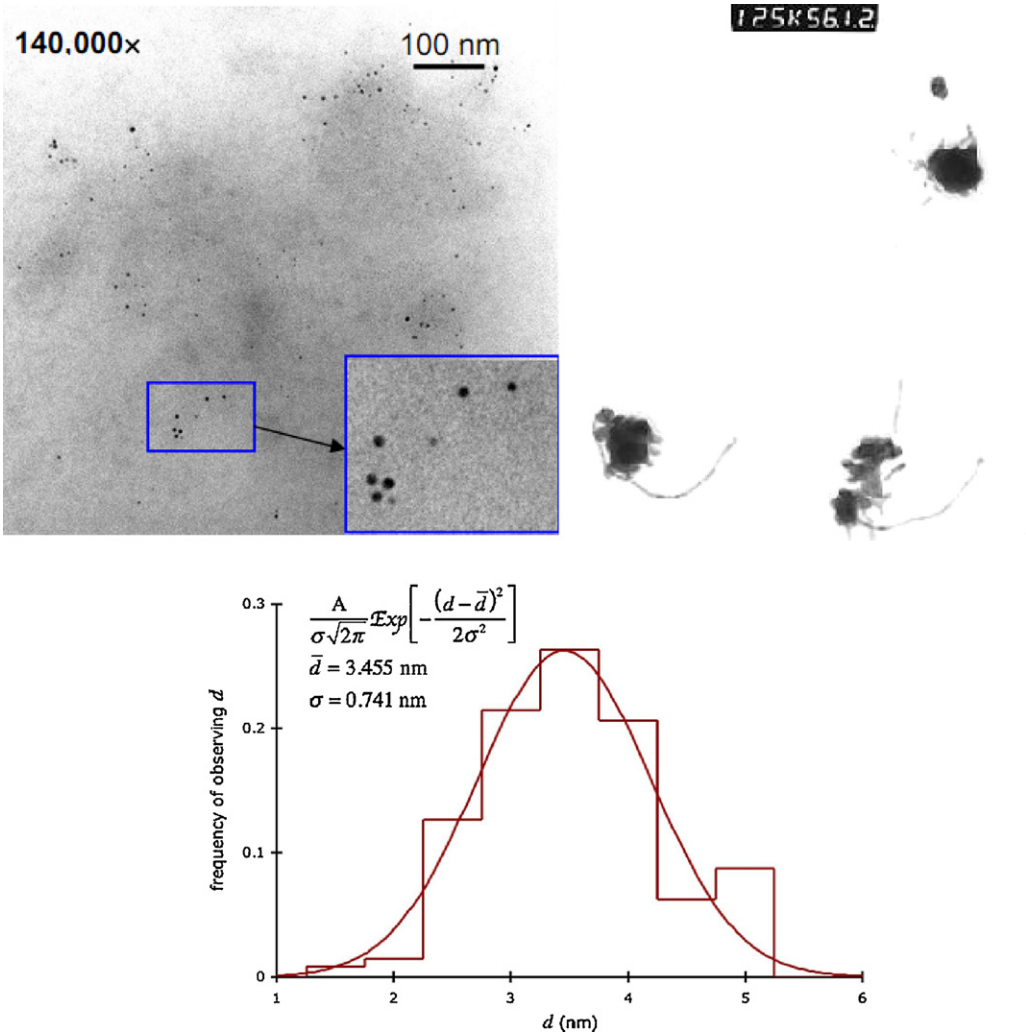

Fig. 5. (Left) TEM image of keratin stabilized nanoparticles. (Right) TEM image showing head-tail structure sometimes encountered. (Bottom) Histogram showing size distribution of keratin stabilized nanoparticles.

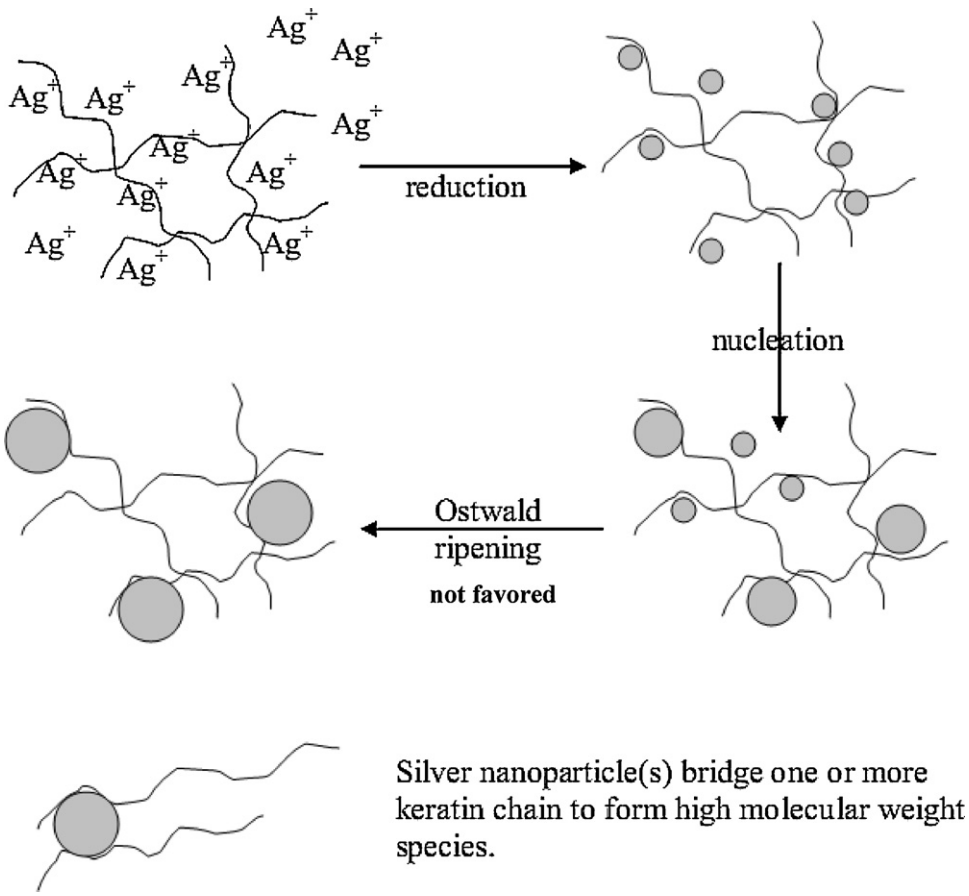

Fig. 6. Formation of silver nanoparticles with keratin chains.

electrostatic interactions. In our system, this presumably occurs at the amide or a free amine based on the FT-IR experimental data. This is referred to as the recognition phase. The next step involves the reduction of the silver ions by sodium borohydride to form silver nuclei which grow by additional reduction of silver nuclei in the solution and deposit on the initially formed nuclei. The nanoparticles can continue to grow over time if conditions are favorable via Ostwald ripening which involves smaller nanoparticles being dissolved due to their high surface energy and the newly dissolved material being accumulated on the larger nanoparticles [33].

To produce nanoparticles at the size indicated by our TEM experiments, the silver products produced by the solvation of unstable nanoparticles are likely captured by adjacent free functional groups on the keratin capping agent, thus limiting Ostwald ripening and preserving a tight size distribution and small particles. We believe that this mechanism can satisfactorily explain the formation of silver nanoparticles in the presence of a keratin stabilizer. A modification is suggested for the formation of the increased molecular weight (>250 kDa) species to allow the silver nanoparticle(s) to act as bridges between keratin hydrolysate moieties. This process is illustrated in Fig. 6.

Ostwald ripening is known to be enhanced at higher temperatures, thus making the ratio of metal cation:stabilizer (capping agent) and the reaction temperature important parameters if smaller nanoparticles are preferred [28]. Future studies will investigate the range of sizes obtainable in this system by altering the reaction conditions to either favor Ostwald ripening (increase silver to keratin ratio, higher temperatures) or favor the formation of smaller nanoparticles (decrease silver to keratin ratio, lower temperatures). pH is another interesting parameter we will explore in future studies as performing these experiments at higher pH values could yield fascinating results on nanoparticle size and shape due to further functionality opening up due to some chemical groups with larger p*K*a values becoming available [34].

The tight size distribution combined with a small (3.5 nm) average size may make these nanoparticles advantageous with respect to their antimicrobial properties. In a 2006 report published by Panacek et al., the researchers reported the synthesis of a variety of silver nanoparticles ranging in size from 25 to 450 nm [35]. They concluded that the smallest nanoparticles in their series had the most pronounced effect, likely due to their increased surface area. Of recent interest is the fact that the researchers demonstrated efficacy against methicillin-resistant *Staphylococcus Aureus*. Furthermore, other studies using STEM and EDS showed silver nanoparticles not only at the cell membrane surface but also inside the bacteria [36]. If diffusion of silver nanoparticles into the bacteria is indeed helpful, smaller nanoparticles with higher surface areas should have an advantage. The antimicrobial activity of our materials is outside the scope of the current investigation.

3.6. Stability of keratin stabilized nanoparticles

Unfortunately, silver nanoparticles prepared using desirable commercially available polymers such as polyvinyl alcohol (PVA) and other small molecules have rarely demonstrated ideal stability for commercialization [17]. The lack of stability may either be a result of oxidation, the inability to resuspend them from a powder or a tendency to irreversibly aggregate over a relatively short time. In comparison, the shelf life of prepared aqueous suspensions of keratin capped nanoparticles appears to be excellent. Samples have been stored as aqueous suspensions on shelves at

room temperature with no signs of precipitation or changes in the SPR absorbance for time periods exceeding six months. Furthermore, the morphology of the formed nanoparticles appears to be unaffected by prolonged excitation of the SPR band. We hypothesize that the increased stability is due to the versatility of the keratin stabilizer. If a fraction of the particles are acting as bridges between keratin chains and others are simply entangled within the polymeric stabilizer, then the nanoparticles will not have sufficient interaction to aggregate. Furthermore, if some of the smaller particles are dissolved, the ions could simply adsorb to an available Lewis base moiety instead of depositing on existing nanoparticles (Ostwald ripening). For small molecule stabilizers like that of the citrate anion, Mirkin and co-workers reported the photoinduced conversion of nanospheres into marked triangular nanoprisms using ordinary overhead fluorescent lighting over a time period of several days [5]. This morphology change is marked by a shift in the λ_{max} of the suspension as well as the appearance of a second strong absorption band. No change in the UV–vis spectrum could be observed after several days of irradiating the keratin stabilized nanoparticle suspensions with a 60 W compact fluorescent bulb or after long term shelf storage. This supports the hypothesis that the nanoparticles strongly interact with the keratin stabilizer (confirmed by IR), or fragmented silver nanoclusters being quickly adsorbed by adjacent keratin free functional groups.

We have stored the material as lyophilized powders on the shelf for several months and reconstituted them, observing no shift in the λ_{max} of the SPR band. The importance of the observed stability in suspension and the ability to reconstitute our particles from a powder cannot be overstated. This will allow the particles to be easily integrated into consumer goods such as plastics, paints, and a wide variety of other products. Furthermore, the photostability of the suspensions will make keratin capped nanoparticles more desirable.

A further advantage of using a large molecular weight capping agent is that we have found that the nanoparticle product can be purified easily using common cellulose dialysis membranes. No change in color intensity or UV–vis spectrum was observed during the course of dialysis.

4. Conclusions

Silver nanoparticles showing a unimodal Gaussian distribution have been produced using a keratin hydrolysate stabilizer. The average diameter of the particles is $3.5\,nm \pm 0.7\,nm$. The molecular weight of the capping agent is predominantly 6.5 kDa or less as determined by gel electrophoresis. Upon formation of nanoparticles, an intense band is observed from gel electrophoresis corresponding to a molecular mass >250 kDa. The increase in molecular weight is attributed to silver nanoparticles acting as cross-links between keratin chains. Circular dichroism spectroscopy revealed that the capping agent showed only a disordered or random secondary structure and that the formation of nanoparticles showed no observable effect on the macromolecular conformation. FT-IR results suggest that the silver interacts with the amide region of the extracted protein as well as the hydroxyl region as shown by shifts in the frequency of these modes. Additionally, FT-IR analysis shows that the keratin caps the silver nanoparticles as evidenced by broadening of the amide I region. Most importantly, the keratin capped silver nanoparticles are extremely stable, remaining suspended for an indefinite time exceeding six months at ambient conditions in aqueous media. The keratin capped particles as a suspension do not form triangular nanoprisms as reported for citrate capped nanoparticles by Mirkin et al. under visible light irradiation [23]. The nanoparticle suspension can be processed into a powder via lyophilization which can be stored indefinitely and is easily resuspended in water, suggesting that the keratin capping agent protects the nanoparticles from oxidative etching, agglomeration and the polar functionalities/salt groups aid in dispersion. This synthesis is simple, highly reproducible and could result in a multitude of versatile biocompatible antimicrobial coatings by utilizing the rich chemistry of keratin. Future studies will investigate the antimicrobial efficacy of this material under various representative situations and the transfer of this material to textiles.

Acknowledgement

The authors would like to thank Paul Pierlott for his photography of the lyophilized powder.

References

[1] A. Aluigi, M. Zoccola, C. Vineis, C. Tonin, F. Ferrero, M. Canetti, Int. J. Biol. Macromol. 41 (2007) 266–273.
[2] (a) J.M. Cardamone, Int. J. Biol. Macromol. 42 (2008) 413–419;
(b) J.M. Cardamone, Textile Res. J. 77 (2007) 214–221;
(c) J.M. Cardamone, J.G. Philips, Textile Res. J. 77 (2007) 277–283;
(d) J.M. Cardamone, J.J. Martin, Macromol. Symp. 272 (2008) 161–166.
[3] J. Koga, K. Kawaguchi, E. Nishio, K. Joko, J. Appl. Polym. Sci. 37 (1989) 2131–2140.
[4] G.J. Dias, P.V. Peplow, A. McLaughlin, F. Teixeira, R.J. Kelly, J. Biomed. Mater. Res. A 92 (2010) 513–520.
[5] (a) R. Jin, C. Cao, E. Hao, G.S. Métraux, G.C. Schatz, C.A. Mirkin, Nature 425 (2003) 487–490;
(b) R. Jin, Y. Cao, C.A. Mirkin, K.L. Kelly, G.C. Schatz, J.G. Zheng, Science 294 (2001) 1901–1903;
(c) K.L. Kelly, E. Coronado, L.L. Zhao, G.C. Schatz, J. Phys. Chem. B 107 (2003) 668;
(d) C. Xue, X. Chen, S.J. Hurst, C.A. Mirkin, Adv. Mater. 19 (2007) 4071–4074;
(e) C. Xue, C.A. Mirkin, Angew. Chem. Int. Ed. 46 (2007) 2036–2038.
[6] Y. Wang, Q. Yang, G. Shan, C. Wang, J. Du, S. Wang, Y. Li, X. Chen, X. Jing, Y. Wei, Mater. Lett. 59 (2005) 3046–3049.
[7] Y. Gogotsi, Nanomaterials Handbook, CRC, Boca Raton, Florida, 2006.
[8] C. Lofton, W. Sigmund, Adv. Funct. Mater. 15 (2005) 1197–1208.
[9] C.N. Lok, C.M. Ho, R. Chen, Q.Y. He, W.Y. Yu, H. Sun, P.K.H. Tam, J.F. Chiu, C.M. Che, J. Proteome Res. 5 (2006) 916–924.
[10] P. Dibrov, J. Dzioba, K.K. Gosink, C.C. Hase, Antimicrob. Agents Chemother. 46 (2002) 2668–2670.
[11] P. Kar, M.J. Misra, Chem. Technol. Biotechnol. 79 (2004) 1313–1319.
[12] G. Freddi, M. Tsukada, H.J. Shiozaki, J. Appl. Polym. Sci. 71 (1999) 1573–1579.
[13] A.N. Syed, K. Ahmad, U.S. 5641477 (1997).
[14] E. Tolgyesi, F. Fang, in: Orfanos, Montagna, Stuttgen (Eds.), Hair Research, Springer-Verlag, Berlin/Heidelberg, 1981, p. 116.
[15] (a) P.E. Laibinis, G.M. Whitesides, D.L. Allara, Y.T. Tao, A.N. Parikh, R.G. Nuzzo, J. Am. Chem. Soc. 113 (1991) 7152;
(b) J.C. Love, L.A. Estroff, J.K. Kriebel, R.G. Nuzzo, G.M. Whitesides, Chem. Rev. 105 (2005) 1103.
[16] L. Yang, R. Xing, Q. Shen, K. Jiang, F. Ye, J. Wang, Q. Ren, J. Phys. Chem. B 110 (2006) 10534–10539.
[17] N. Singh, P.K. Khanna, Mater. Chem. Phys. 104 (2007) 367–372.
[18] K. Ishizu, H. Kakinuma, K. Ochi, S. Uchida, M. Hayashi, Polym. Adv. Technol. 16 (2005) 834.
[19] C.R.K. Rao, D.C. Trivedi, Synth. Met. 155 (2005) 324–327.
[20] S. Li, Y. Shen, A. Xie, X. Yu, L. Qiu, L. Zhang, Q. Zhang, Green Chem. 9 (2007) 852–858.
[21] S.S. Shankar, A. Rai, A. Ahmad, M. Sastry, Biotechnol. Prog. 19 (2003) 1627.
[22] C.R. Cantor, P.R. Schimmel, Biophysical Chemistry Part II: Techniques for the Study of Biological Structure and Function, W.H. Freeman and Company, San Francisco, 1980, p. 349–408.
[23] (a) C.A. Mirkin, R.L. Letsinger, R.C. Mucic, J.J. Storhoff, Nature 382 (1996) 607–609;
(b) R.C. Mucic, J.J. Storhoff, C.A. Mirkin, R.L. Letsinger, J. Am. Chem. Soc. 120 (1998) 12674–12675.
[24] C.N.R. Rao, S.R.C. Vivekchand, K. Biswas, A. Govindaraj, Dalton Trans. (2007) 3728–3749.
[25] E.A. Hauser, J.E. Lynn, Experiments in Colloid Chemistry, McGraw-Hill, New York, 1940, p. 18.
[26] C. Burda, X. Chen, R. Narayanan, M.A. El-Sayed, Chem. Rev. 15 (2005) 735.
[27] (a) X.S. Fang, C.H. Ye, X.S. Peng, Y.H. Wang, Y.C. Wu, L.D. Zhang, J. Mater. Chem. 13 (2003) 3040;
(b) X.S. Fang, C.H. Ye, L.D. Zhang, J.X. Zhang, J.W. Zhao, P. Yan, Small 1 (2005) 422;
(c) X.S. Fang, C.H. Ye, L.D. Zhang, Y.H. Wang, Y.C. Wu, Adv. Funct. Mater. 15 (2005) 63;
(d) X.S. Fang, L.D. Zhang, J. Mater. Sci. Technol. 22 (2006) 1–18.
[28] J.T. McCann, D. Li, Y. Xia, J. Mater. Chem. 15 (2005) 735.

[29] (a) B. Mayers, Y. Xia, J. Mater. Chem. 12 (2002) 1875;
(b) U. Jeong, P.H.C. Camargo, Y.H. Lee, Y. Xia, J. Mater. Chem. 16 (2006) 3893.
[30] F. Kim, S. Connor, H. Song, T. Kuykendall, P. Yang, Angew. Chem. Int. Ed. 43 (2004) 3673–3677.
[31] C.J. Murphy, A.M. Gole, S.E. Hunyadi, C.J. Orendorff, Inorg. Chem. 45 (2006) 7544–7554.
[32] M. Yamamoto, Y. Kashiwagi, M. Nakamoto, Langmuir 22 (2006) 8581–8586.
[33] A.B. Denison, L.J. Hope-Weeks, R.W. Meulenberg, L.J. Terminello, in: M. DiVentra, S. Evoy, J.R. Heflin Jr. (Eds.), Introduction to Nanoscale Science and Technology, Springer Science and Business Media LLC, New York, 2004, pp. 183–198.
[34] L. Lundblad, Techniques in Protein Modification, CRC Press, Boca Raton, 1994, p. 1–9.
[35] A. Panacek, L. Kvitek, R. Prucek, M. Kolar, R. Vecerova, N. Pizurova, V. Sharma, T. Nevecna, R. Zboril, J. Phys. Chem. B 110 (2006) 16248–16253.
[36] J.R. Morones, J.L. Elechiguerra, A. Camacho, K. Holt, J. Kouri, J.T. Ramirez, M.J. Yacaman, Nanotechnology 16 (2005) 2346.